


FULL PAPER

Open Access



Propagation characteristics of sporadic E and medium-scale traveling ionospheric disturbances (MSTIDs): statistics using HF Doppler and GPS-TEC data in Japan

Ryo Matsushima¹, Keisuke Hosokawa^{1*} , Jun Sakai¹, Yuichi Otsuka², Mitsumu K. Ejiri^{3,4}, Michi Nishioka⁵ and Takuya Tsugawa⁵

Abstract

We carried out a statistical analysis of the propagation characteristics of Es and Medium-Scale Traveling Ionospheric Disturbances (MSTIDs) by combining data of HF Doppler (HFD) sounder and Total Electron Content (TEC) obtained from the GPS receivers of GEONET (GPS-TEC) for 4 years from 2014 to 2017. We made use of Es reflection data from the HFD receivers in Sugito, Saitama (36.0°N, 139.7°E), Fujisawa, Kanagawa (35.3°N, 139.5°E), and Sugadaira, Nagano (36.4°N, 138.3°E) in Japan. By using this triangle observation, we succeeded in deriving the horizontal speed and direction of the motion of Es. In addition, we estimated the phase velocity of MSTIDs observed in the simultaneously obtained maps of GPS-TEC with the same triangle observation procedure. The speeds of Es and MSTIDs were commonly less than 100 m/s in most cases and their propagation direction was predominantly southwestward. This result is consistent with the statistical characteristics of nighttime MSTIDs observed in the previous studies. More importantly, good correspondence between the propagation characteristics of the two phenomena at two different altitudes confirms that Es and MSTIDs move in tandem with each other, further suggesting that Es in the E region plays an important role in the generation and propagation of MSTIDs in the F region.

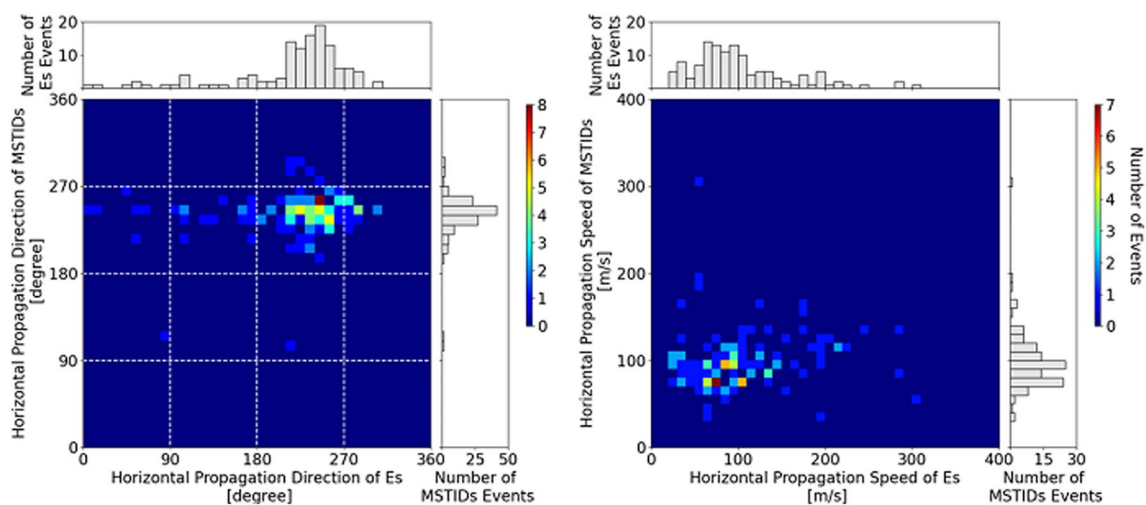
Keywords: Ionosphere, Sporadic E (Es), Medium-scale traveling ionospheric disturbances (MSTIDs), HF Doppler (HFD) sounding, E–F coupling

*Correspondence: keisuke.hosokawa@uec.ac.jp

¹ University of Electro-Communications, Chofugaoka 1-5-1, Chofu, Tokyo 182-8585, Japan

Full list of author information is available at the end of the article

Graphical Abstract



Main text

Introduction

Sporadic E (Es) is one of the outstanding phenomena in the mid-latitude E region ionosphere during summer months (e.g., Haldoupis et al. 2007). Es is a thin and dense layer of ionization mainly composed of metallic ions originating from meteorites (Haldoupis 2011). It has been suggested that the vertically thin structure of Es is produced through a concentration of metallic ions caused by the vertical shear of zonal neutral wind (Whitehead 1961), which has been known as “wind shear theory.” Extremely high electron density within Es is known to reflect high-frequency (HF) and very high-frequency (VHF) radio waves, sometimes above 100 MHz, when the wave incidence is highly oblique to the ionosphere (Sakai et al. 2020). Such an Es reflection often causes radio interferences, for example, to aeronautical navigation systems (Sakai et al. 2019). For these reasons, Es has been studied intensively since 60’s by combining various ground-based radio instruments such as ionosondes. Recently, Maeda and Heki (2014) employed data of Total Electron Content (TEC) obtained from the GPS receivers of GEONET (GPS-TEC) in Japan and demonstrated a 2D frontal structure of Es elongating more in the zonal direction. Kurihara et al. (2010) observed Es at night with the Magnesium Ion Imager (MII) on the sounding rocket launched from the Uchinoura Space Center in Kagoshima, and confirmed that the horizontal structure of Es at night had a frontal structure extending from northwest to southeast.

In the recent a few decades, nighttime Es has been studied in close relationship with Medium-Scale Traveling Ionospheric Disturbances (MSTIDs; Hunsucker 1982), which are also one of the most prominent phenomena in the mid-latitude F region ionosphere. MSTIDs during nighttime are known as wave-like disturbances, whose wavefronts are elongated from northwest to southeast and propagate southwestward (e.g., Saito et al. 1998; Ogawa et al. 2009). MSTIDs are observed not only during nighttime but also during daytime, especially in winter. Since the characteristics of MSTIDs (e.g., propagation direction and local time variation) during daytime and nighttime are noticeably different, separate mechanisms have been proposed for explaining their generation. For example, Otsuka et al. (2013) investigated the statistical properties of MSTIDs using GPS-TEC observations in the European sector and reported significant differences between the nighttime and daytime MSTIDs. The daytime MSTIDs are frequently observed in winter and propagate mostly southeastward. In addition, the direction of propagation rotates from southeastward to southwestward (Otsuka et al. 2011). According to these previous studies, the daytime MSTIDs are manifestations of atmospheric gravity waves (AGWs; Hines 1960; Hooke 1968).

In contrast, the nighttime MSTIDs occur frequently in the Asian/Oceanian (eastern Pacific/American) region is higher during June (December) solstice (Park et al. 2010). In addition, the nighttime MSTIDs are often observed with Es (e.g., Hysell et al. 2011; Helmboldt 2016), which

implies that the nighttime MSTIDs are generated by plasma instabilities (i.e., combination of Es instability and Perkins instability) in the E and F region coupling system (Cosgrove and Tsunoda 2004). Several studies tried to observe Es and MSTIDs at the same time. For example, Otsuka et al. (2008) compared the daily activities of Es and MSTIDs which were, respectively, observed by an ionosonde and GPS-TEC measurements in Japan. They demonstrated that the seasonal and day-to-day variations of the occurrence of MSTIDs is surely correlated with the appearance of Es. This result suggested a close connection between Es and F region phenomena via magnetic field line. However, chances of simultaneous observations of E and F region phenomena have still been limited; thus, the detailed dynamical characteristics of Es and MSTIDs have not yet been compared. Recent numerical simulations have suggested that Es itself or Es instability plays an important role in generating MSTIDs during nighttime (e.g., Yokoyama et al. 2009; Yokoyama and Hysell 2010).

Recently, Ejiri et al. (2019) observed the activity of Es by using a Lidar system in Tachikawa (35.7°N, 139.4°E), Tokyo and compared it with the variation of MSTIDs as visualized by GPS-TEC. In their study, the density of Es was estimated by using the column abundance of metallic ions (Ca^+ , Fe^+ , etc., Ca^+ in their case) within Es. They found that the time series of GPS-TEC variation and Ca^+ column abundance are very similar during the interval of interest, suggesting that Es and MSTIDs are closely connected with each other. However, the Lidar observation of Es by Ejiri et al. (2019) was a single point measurement over Tachikawa, Tokyo; thus, it was difficult to compare the propagation characteristics of Es and MSTIDs. In this study, we tried to derive the horizontal propagation speeds and directions of Es and MSTIDs by using multi-point observations of HF Doppler (HFD) sounding system and GPS-TEC, and then compared them in a statistical fashion. Based on the statistics, we discuss the E–F coupling process to further understanding the relation between the generation of MSTIDs and dynamical characteristics of Es.

Observation

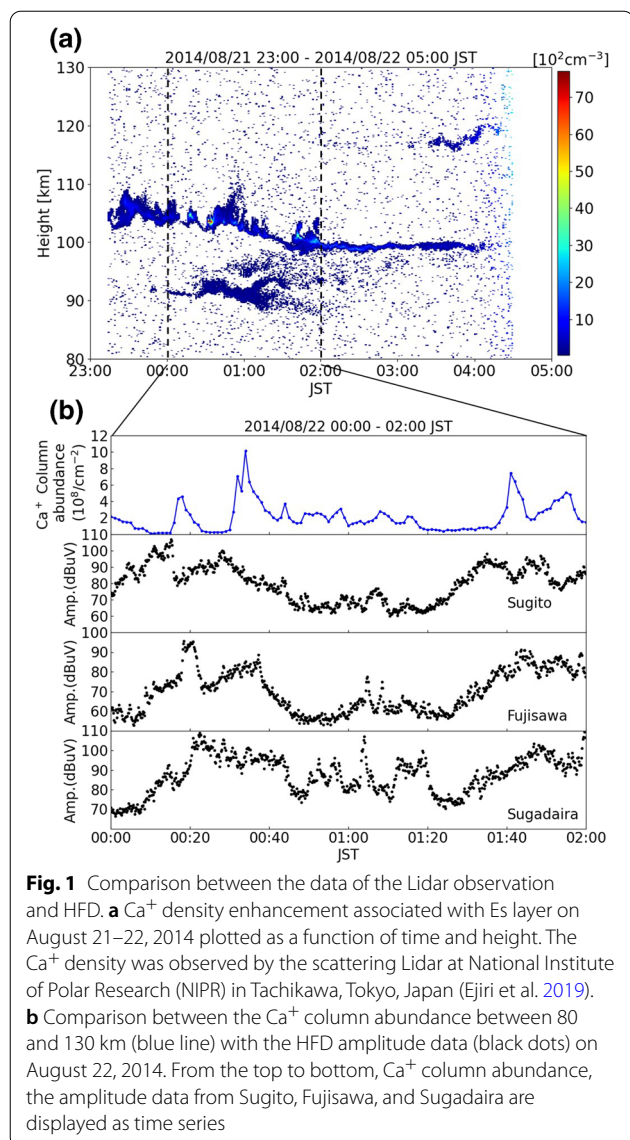
In this study, we mainly use data from the HFD sounding system in Japan for detecting Es in the E region and those from the GPS-TEC of GEONET for observing MSTIDs in the F region. Here, we briefly introduce these radio observation techniques for measuring two different ionospheric phenomena at two different altitudes.

Ionospheric observations using the HFD sounding (Watts and Davies 1960) started at around the late 50s and early 60s and have been carried out in various latitudinal/longitudinal areas for precise measurements

of ionospheric disturbances, such as MSTIDs and AGWs (e.g., Vincent and Reid 1983). In this study, we employ data from an HFD system currently operative in Japan (HFDOPE: <http://gwave.cei.uec.ac.jp/~hfd>). The HFDOPE system transmits radio waves at two frequencies (5006 and 8006 kHz) from a transmitter (Tx station) in Chofu, Tokyo (35.7°N, 139.5°E). Those transmitted waves are reflected by the ionosphere with a Doppler shift in frequency and are observed by receivers deployed in a number of Rx stations in Japan. The original sampling rate at the Rx stations is 100 Hz and we derive the amplitude and Doppler frequency every 10 s with an FFT (Fast Fourier Transformed) windows of ~40-s duration (4096 samples); thus, the temporal resolution of the Doppler shift data product is 10 s.

In order to detect the appearance of Es, we employ the amplitude data (not the Doppler shift data) at 8006 kHz at several stations in the eastern part of Japan (near Tokyo area). By applying a cross-correlation analysis to the amplitude data from closely distributed multiple Rx stations, we derive the propagation characteristics of Es. Before performing such an analysis, we have evaluated if the appearance of Es can be identified by the amplitude data at 8006 kHz by comparing the HFD data with the Es observation by the Lidar system as introduced by Ejiri et al. (2019). Figure 1a shows the Ca^+ Lidar observations of Es layer on August 21, 2014. A thin layer of dense Ca^+ (i.e., Es layer) is observed at around 100–110 km altitudes. The top panel of Fig. 1b shows the time series of the Ca^+ column abundance between 80 and 130 km derived from Fig. 1a. The bottom three panels of Fig. 1b show the HFD amplitude in the same interval from three Rx stations in Sugito, Fujisawa, and Sugadaira. Although the temporal variations of the Ca^+ column abundance and HFD data are slightly different, an overall one-to-one correspondence is observed between the peaks.

When closer looking at the time series of the HFD data from Sugito, we can identify four characteristic peaks, the peaks at about 00:10, 00:25, 01:35, and 01:50 JST (JST/LT: Japan Standard Time). These four peaks can be found in the HFD data from the other two sites and also in the data of Ca^+ column abundance from the Lidar. In particular, the peaks in the Ca^+ column abundance data are located at the time of the peaks in the HFD data from Fujisawa. This is simply because the geographic locations of the Fujisawa and Tachikawa (where observation of Ca^+ Lidar is conducted) are relatively close. This good correspondence suggests that the amplitude of the HFD signal increases when a dense Es passes through the reflection point; thus, the amplitude of the HFD data can be used as a proxy for the density of Es. Comparing the Ca^+ column abundance data with the data from the other two



HFD sites (Sugito and Sugadaira), there is a time delay of 5–10 min in timing of the peaks. These systematic delays were caused by the propagation of Es structure through the sensing areas of the Lidar and HFD observations, where the characteristic HFD peaks are detected in the order of Sugito, Fujisawa, and Sugadaira. Considering the geometry of the three points, Es should have propagated in the southwest direction. The detailed analysis of this event, including the MSTIDs observed simultaneously, will be introduced in the next section. Such an analysis is needed to evaluate if the multi-point HFD observation is able to estimate the propagation speed and direction of the Es event introduced by Ejiri et al. (2019), and to further confirm the reliability of the derived propagation parameters.

To detect MSTIDs and estimate their propagation characteristics, we also employ the Total electron content (TEC) data, derived for more than 1000 two-frequency GPS receivers of GEONET in Japan. We employed the GPS-TEC data provided by the DRAWING-TEC database (<https://aer-nc-web.nict.go.jp/GPS/DRAWING-TEC/>). To detect small fluctuations in TEC caused by the propagation of MSTIDs, we made use of the 1-h detrended GPS-TEC data obtained from each pair of satellite and receiver, where the background trend for subtraction is calculated by averaging data in a 60-min window whose center is located at the time of interest (Tsugawa et al. 2007). After detrending, the slant TEC was converted to vertical TEC by multiplying a slant factor. The obtained vertical TEC values were mapped onto a map binned with horizontal cells whose resolution is $0.15^\circ \times 0.15^\circ$ in latitude and longitude by assuming the altitude of Ionospheric Pierce Point (IPP) at 300 km. The TEC data within each horizontal cell were then averaged. In the later part of the paper, we make a time series of TEC data at the reflection points of HFD observations for the cross-correlation analyses. When carrying out such analyses, we use the averaged TEC data at a cell nearest to the reflection point of HFD. In such a case, we do not need to consider the motion of IPPs in time.

There is a possibility that the GPS-TEC values derived through the above-mentioned procedure are influenced by the appearance of Es. By considering that Es is much thinner in altitude, such a contribution would be negligible in most cases (the total contribution is well less than 1 TECU for cases of daytime Es, e.g., Maeda and Heki 2015) since MSTIDs exist in much denser F region. As will be mentioned in the next section, we set a threshold of 1 TECU (TEC Unit: $1.0 \times 10^{16} \text{ m}^{-2}$) for the detection of MSTIDs from the GPS-TEC data; thus, the variation of GPS-TEC is mainly due to the contribution from MSTIDs. We attach a movie of GPS-TEC data during MSTIDs created by assuming the IPP at 300 km to this paper. If the assumption of IPP at 300 km is incorrect or there is a significant contribution from the E region, it would be impossible to detect clear wavefronts of MSTIDs as shown in the attached Additional file 1: Movie S1. This supports our assumption that the contribution of Es to GPS-TEC observation is not significant for the nighttime MSTID events. However, Muafiry et al. (2018) demonstrated that the amplitude of TEC enhancement can be larger than 1 TECU for some strong Es events during daytime showing a single frontal structure. This means that the extraction of MSTID from the GPS-TEC data can be affected by the appearance of such extreme Es cases. Thus, we have checked GPS-TEC

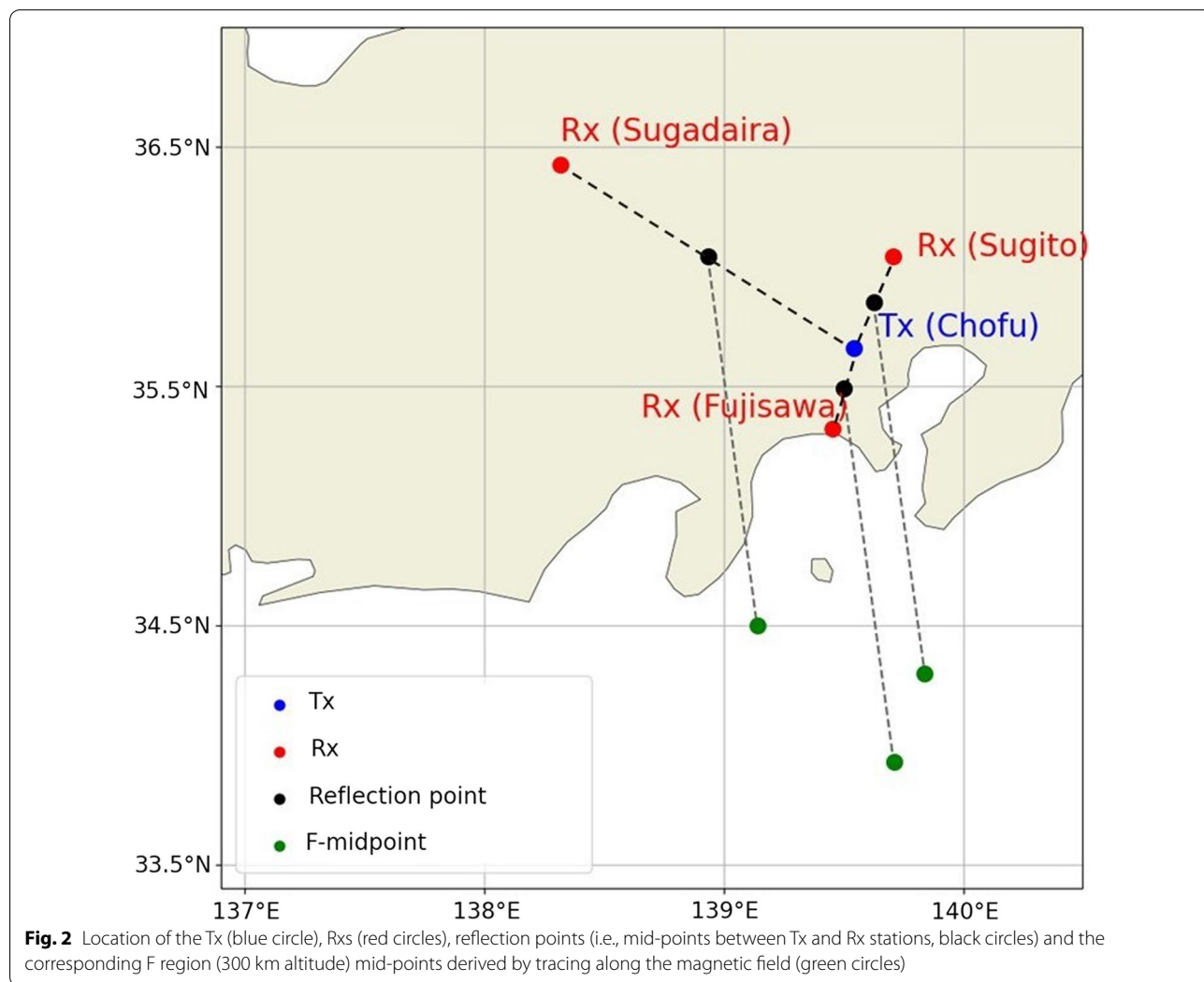
maps during 68 events used for the statistics, which is shown in Fig. 6, and confirmed the existence of multiple frontal structures indicating the propagation of MSTIDs in the F region.

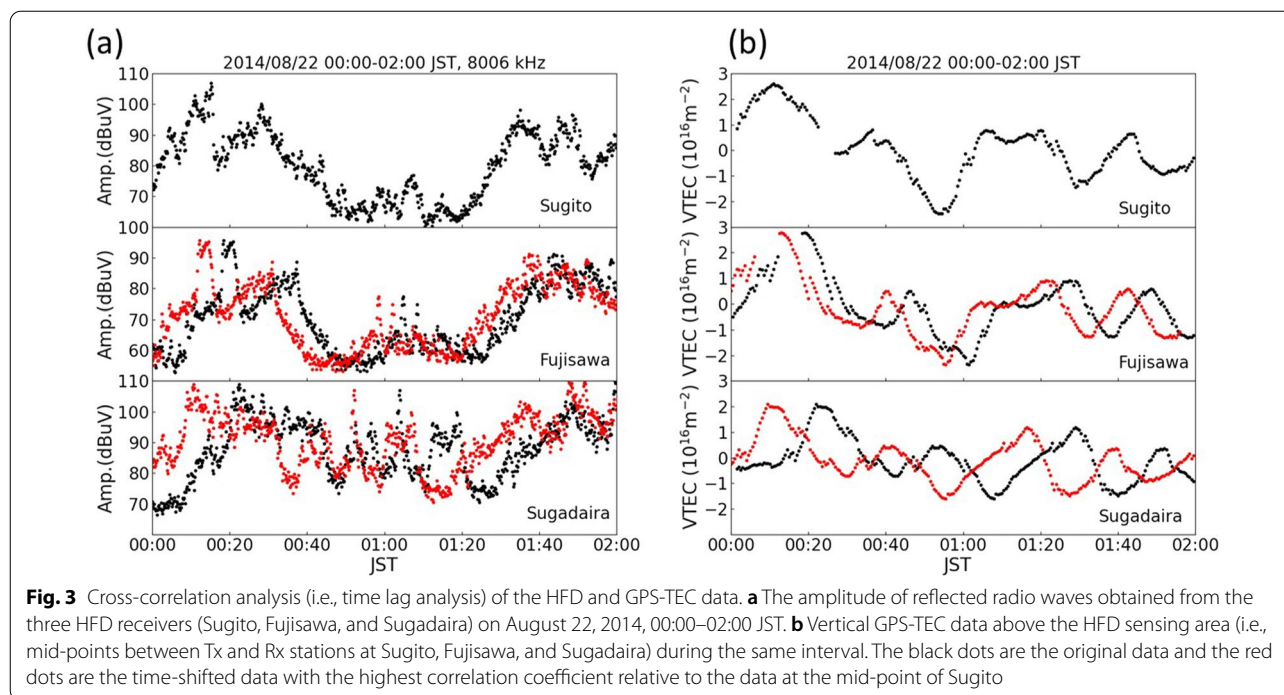
Method and result

We derived the horizontal propagation speeds and directions of Es and MSTIDs, respectively, by using data from the HFD and GPS-TEC observations in Japan. We made use of Es reflection data (the amplitude of reflected radio waves) from the three HFD receivers at Sugito, Saitama (36.0°N, 139.7°E), Fujisawa, Kanagawa (35.3°N, 139.5°E), and Sugadaira, Nagano (36.4°N, 138.3°E) in the eastern part of Japan (Kanto area). Ionospheric reflection of the radio waves generally takes place at the mid-point between the Tx and three Rx stations. Figure 2 shows a map of Kanto area (33.5°–37.0°N, 137.0°–140.5°E), showing the locations of the Tx, Rx stations and three reflection points (i.e., mid-points). Three green points

show the corresponding locations of the mid-points at the altitude of 300 km (F region mid-points) traced along the field line, i.e., F region mid-points of Sugito (34.3°N, 139.8°E), Fujisawa (34.5°N, 139.1°E), and Sugadaira (33.9°N, 139.7°E). This field line tracing was done by using a magnetic field model of IGRF-12 (Thébault et al. 2015). First, to compare the propagation parameters of Es and MSTIDs in a direct manner, we employed the 1-h detrended vertical TEC (dTEC) data at the F region altitude (300 km) immediately above the reflection points (black circles in Fig. 2) of Sugito, Fujisawa, and Sugadaira.

We calculated the propagation speeds and directions of events by estimating time lags between time series from three points. These time lags are primarily introduced by the horizontal propagation of a linear (i.e., frontal) structure passing through the three mid-points sequentially. Figure 3 demonstrates how the time lags were estimated from the HFD and GPS-TEC data from three points. Figure 3a shows the HFD data from the three Rx stations

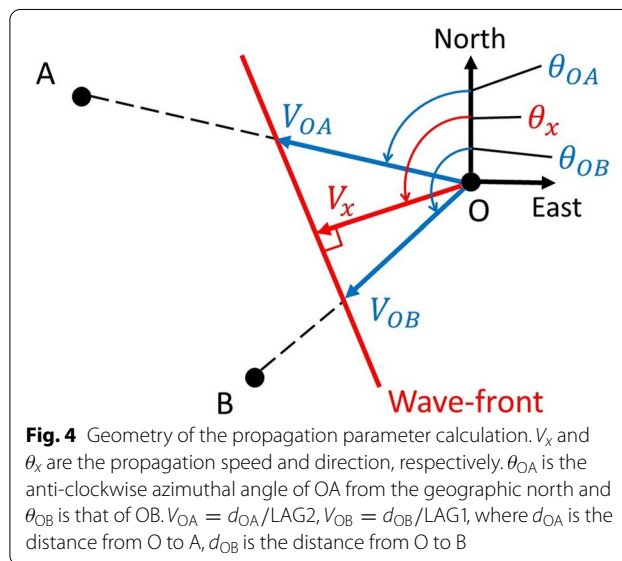




during a 2-h interval from 00 to 02 JST on August 22, 2014. In all the panels, the black lines indicate the original data showing variations of 8006 kHz amplitude caused by the passage of Es across the reflection points (Top: Sugito, Middle: Fujisawa, Bottom: Sugadaira).

In the bottom two panels of Fig. 3a, the red lines indicate time-shifted data with a lag having the highest correlation coefficient with the original time series from Sugito. When estimating these time lag values, cross-correlation analyses were carried out, by using data from Sugito as a reference, with a shifting time window of 10 s. Here, the duration of the window for the cross-correlation analysis was 60 min, including 30-min intervals before and after the time of interest. Figure 3b shows the GPS-TEC data obtained above the three mid-points of HFD observation (Top: Sugito, Middle: Fujisawa, Bottom: Sugadaira). The format of the plots (i.e., the meaning of the black lines and red lines) is same as in Fig. 3a. The dTEC data were obtained every 30 s, while HFD data were 10 s; thus, the shifting time during the cross-correlation analysis was set to 30 s, but the same duration of the window was used for processing of both the data.

The comparison of the red lines in the bottom two panels of Fig. 3a and b (shifted time series) with the black line in the top demonstrates that the timings of the peaks are similar among them, indicating that the Es or MSTID structure causing these variations propagated through the stations without significant change of its spatial structure. As a next step, time lags will be used for calculating the propagation speeds and directions of events.



Here we introduce how we calculated the propagation direction and speed of Es/MSTID from the estimated time lag values. Figure 4 schematically illustrates the geometry of the calculation process, where point O corresponds to the mid-point of Sugito, point A to Sugadaira, and point B to Fujisawa. It is noted that, in Fig. 4, the wavefront of Es/MSTID is described to propagate in the southwest direction, but this is only for the sake of explanation. When we calculated the time lags between

Sugito and the other two points, we shifted the data back and forth by 30 min (i.e., total 1 h surrounding the time of interest) and pick up a lag having maximum cross-correlation coefficient. Therefore, it is possible to calculate the propagation parameters even for cases where the receivers in Sugadaira and Fujisawa detected the signatures first. That is, the current method supports the detection of all the propagation direction.

As demonstrated in Fig. 3, two time lag values are estimated from the cross-correlation analyses: LAG1 between O (Sugito) and B (Fujisawa) and LAG2 between O and A (Sugadaira). By using these two time lags, we calculated V_{OA} and V_{OB} , which are, respectively, apparent speeds of wavefront along OA and OB (i.e., $V_{OA} = d_{OA}/LAG2$, $V_{OB} = d_{OB}/LAG1$, where d_{OA} is the distance from O to A and d_{OB} is that from O to B). By using these two apparent speeds, we have derived the propagation direction of the wavefront, θ_x , by using the following equation:

$$\tan \theta_x = \frac{V_{OA} \cos \theta_{OA} - V_{OB} \cos \theta_{OB}}{V_{OA} \sin \theta_{OA} - V_{OB} \sin \theta_{OB}}. \quad (1)$$

In a similar manner, we have calculated the propagation speed, V_x , by using the following equations:

$$V_x = \frac{V_{OA} V_{OB} \sin(\theta_{OA} - \theta_{OB})}{\sqrt{V_{OA}^2 + V_{OB}^2 - 2V_{OA} V_{OB} \cos(\theta_{OA} - \theta_{OB})}}. \quad (2)$$

Note here that θ_x , θ_{OA} , and θ_{OB} are depicted as the anticlockwise azimuthal angle from the geographic north in Fig. 4, but the propagation directions that follow are expressed in azimuthal angles with north as 0 degree.

First, we calculated the propagation speeds and directions of the Es and MSTID event introduced in the “**Observation**” section (Fig. 1). The data used for the analysis are the two-hour time series (black lines) shown in Fig. 3. By using these time series, we estimated the time lags for deriving the propagation characteristics. The estimated time lags in the HFD data were 380 s for the Sugito-Fujisawa pair and 720 s for the Sugito-Sugadaira pair. On the other hand, the time lags in the GPS-TEC data were 360 s for the Sugito-Fujisawa pair and 750 s for the Sugito-Sugadaira pair. By putting these values of time lag into Eqs. (1) and (2), we derived the horizontal propagation speeds and directions of Es and MSTIDs for this particular case, which are summarized in Table 1. The propagation speeds of Es and MSTID were 68.9 m/s and 68.1 m/s, respectively, which are fairly close to each other at around 70 m/s. The propagation directions of Es and MSTID also have similar values, which are 247° for Es and 250° for MSTID, respectively. These propagation parameters indicate that both the Es and MSTIDs in this

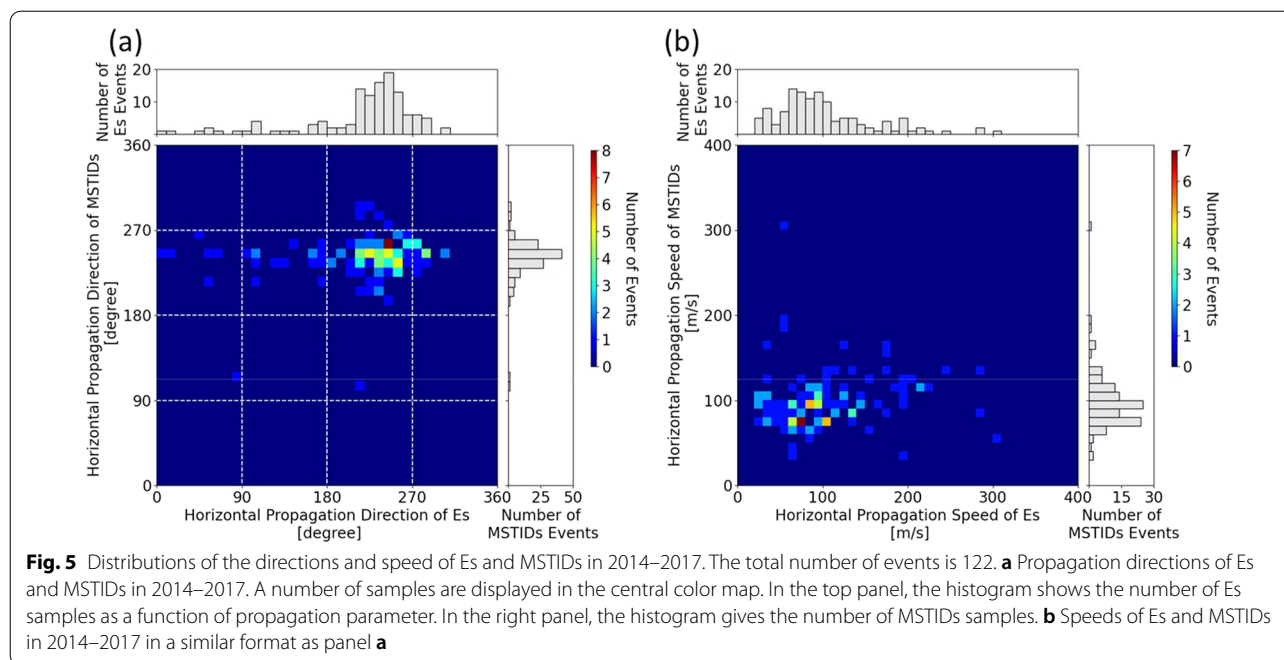
Table 1 Propagation speeds and directions of Es/MSTIDs event on August 22, 2014

	Speed (m/s)	Azimuthal direction (degree)
Es at E region	68.9	247
MSTID at F region	68.1	250

time interval propagated in similar southwestward direction with an almost same speed; that is, their motion was in tandem with each other. Ejiri et al. (2019) observed the MSTID in the same interval by using GPS-TEC and demonstrated that it propagated in the southwest direction with a propagation speed of ~50 m/s. Ejiri et al. (2019) did not perform precise calculation of the propagation speed through a cross-correlation analysis; thus, quantitative comparison cannot be made. At least, however, the order of the propagation speeds is in good agreement with each other, implying the feasibility of the cross-correlation analysis used in this paper. Here, it is noted that the horizontal propagation velocity of Es was not estimated in Ejiri et al. (2019) because the Es was detected by the Lidar as a single point measurement.

As a next step, we analyzed all the cases of simultaneous appearance of Es and MSTIDs during summer months in 4 years from 2014 to 2017 in order to show the statistical characteristics of the propagation parameters. We analyzed all the nighttime data (18–03 JST) from all the months. However, all the extracted Es/MSTIDs events were observed in 5 months from May to September. To extract Es events from the large dataset, we employed the value of foEs from the ionosonde of NICT in Kokubunji, Tokyo (35.7°N, 139.5°E). foEs is the highest frequency of vertical incidence radio waves which can be reflected by Es at the E region altitudes (i.e., critical frequency of Es). For the detection of MSTIDs, we used the amplitude of vertical GPS-TEC data to extract the events. In the course of statistical analysis, if foEs is higher than 8 MHz and the amplitude of detrended GPS-TEC data is larger than 1 TECU, we carried out the automated estimation of propagation speeds and direction of Es and MSTIDs by using the method described in the “**Method and result**” section. We also guarantee simultaneous detection of Es/MSTID at the three points by setting an additional threshold in the correlation coefficient of 0.7 between Sugito and the other two points for both the HFD and GPS-TEC data.

In the statistics, if the foEs value at a specific time is higher than 8 MHz, we estimate the propagation parameters using 2 h of HFD data surrounding the central time when the foEs value is picked up. The foEs values are obtained every 15 min; thus, the propagation parameters



are also derived every 15 min. The number of all the simultaneous detections of Es/MSTID was 122. Figure 5 shows the distributions of the directions and speed of Es and MSTIDs (i.e., 122 event pairs of Es/MSTIDs). In both the panels, the top and right panels are the histogram showing the number of Es (top) and MSTIDs (right) as a function of propagation parameter. The central color panel shows the distribution of the number of samples as a function of propagation parameters of Es (horizontal axis) and MSTID (vertical axis).

The color panel of Fig. 5a indicates that most of the samples are highly concentrated in the range from 180° to 270°, 81 samples (66% of total) being within this range. This implies that both the Es and MSTID propagated predominantly southwestward. Regarding the propagation speeds, Fig. 5b indicates that most of the samples (78 samples: 64%) are distributed in the range between 50 and 150 m/s, except for some large values of the speed of Es exceeding 200 m/s. The statistics again indicates that the speeds of Es and MSTID have similar values. One thing we need to bear in mind is that the distributions of both the parameters are more scattered for the Es samples. We will discuss the reason for this difference between the samples of Es and MSTIDs in the next section.

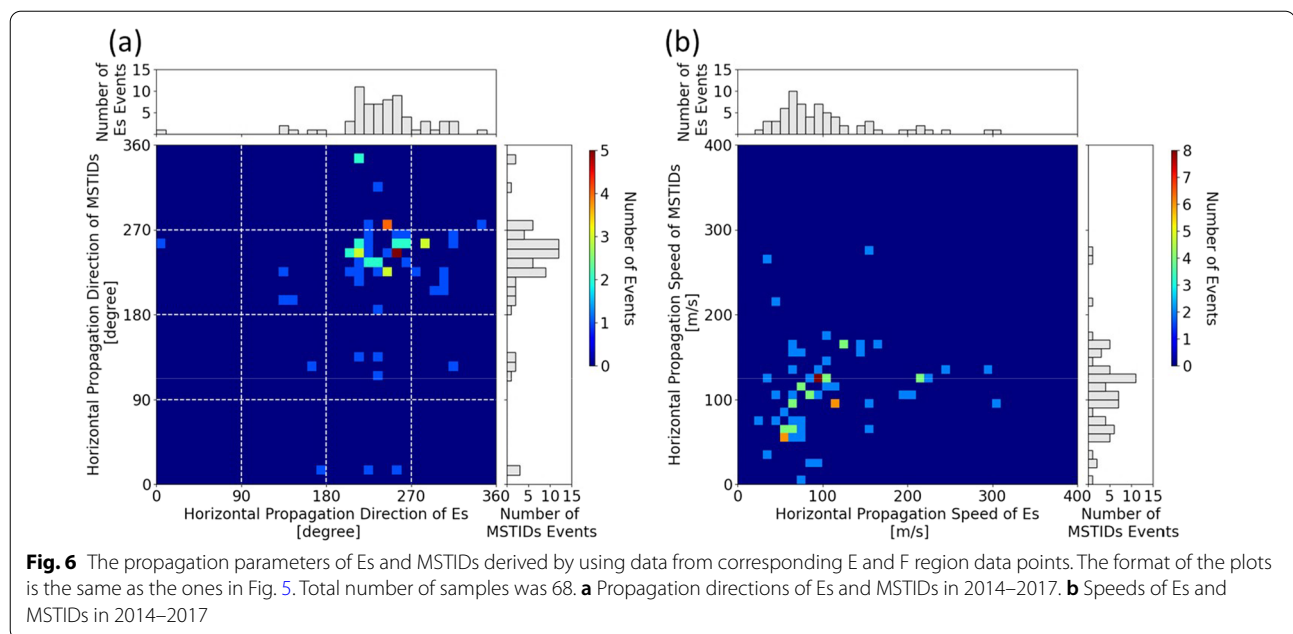
In Fig. 5, we compared the propagation characteristics of Es and MSTIDs which were derived by using simultaneous HFD and GPS-TEC observations at the same three sensing areas (i.e., three mid-points of HFD). In this comparison process, we simply picked up corresponding

GPS-TEC data at the mid-points of the triangle HFD observation. To test the E–F coupling hypothesis (Cosgrove and Tsunoda 2002, 2004) in more rigorous way, however, we should have looked at two locations at two different altitudes (i.e., E and F region) electrically connected along the inclined geomagnetic field line.

Figure 6a and b, respectively, shows the propagation direction and speed of Es and MSTIDs for the direct comparison along the same magnetic flux tube. The format of the plots is the same as the ones in Fig. 5, but here we employed the GPS-TEC data from the green points (F region mid-points) in Fig. 2. The total number of events was reduced to 68, which is about a half the number of cases shown in Fig. 5, because the GPS-TEC data were not available in the sea area for many cases. Although the propagation directions shown in Fig. 6a look more scattered than those in Fig. 5a, we still see a clear concentration between 180° and 270° in the azimuthal direction (southwestward propagation). In Fig. 6b, most of the propagation speeds of Es and MSTID are distributed in the range less than 150 m/s. It is also found that there is a slight linear correlation between the speeds of Es and MSTIDs in the central color map.

Discussion

We studied an event of Es on August 22, 2014, which was previously investigated by Ejiri et al. (2019), and demonstrated that the propagation parameters of Es and MSTIDs are very similar. Particularly, the propagation directions of Es and MSTIDs are southwestward, which



is consistent with the typical propagation direction of MSTIDs during summer nighttime in Japan (Shiokawa et al. 2003; Narayanan et al. 2006). This good correspondence between Es and MSTIDs strongly suggests that MSTIDs at 300 km altitude propagate in tandem with Es at 100 km altitude. To support the result of this case study, we carried out statistics using four years of HFD and GPS-TEC data.

The statistical results shown in Figs. 5 and 6 indicate that the directions of Es and MSTIDs are mainly southwestward, which are consistent with the statistical characteristics of MSTIDs during the nighttime. However, we should bear in mind that these results strongly depend on the assumption in the cross-correlation analysis that Es has a linear horizontal structure passing through the three sensing points sequentially. Such a linear frontal structure of Es was presented by Maeda and Heki (2014) for strong daytime Es events whose foEs exceeded 20 MHz, but it is still unclear if nighttime moderate (> 8 MHz) Es also has a similar frontal structure. Therefore, in order to exclude Es events which do not have a frontal structure, we set a relatively high threshold of 0.7 for the correlation coefficients in the Es extraction process. This allowed us to pick up only the linear frontal Es events for the statistical analysis. In addition, the propagation parameters of Es were derived by using the same method as used for MSTIDs, whose wavefronts can be confirmed visually by using sequential GPS-TEC maps, for example, the one attached to this paper as a movie. This is a strong indication that HFD should have observed the same wavefront of propagating Es in the E region.

As mentioned in previous section, the samples of Es in the color panels of Fig. 5 are more scattered than those of MSTIDs. This tendency is probably due to a difference in the extraction process of Es and MSTIDs in the statistics. We set a threshold in the detrended vertical GPS-TEC value for extracting MSTIDs, which allowed us to extract the phenomenon successfully in most cases. We were not able to employ a similar procedure because the amplitude of the HFD data is more arbitrary due to the changing propagation conditions. Thus, instead, we used the foEs data from near-by ionosonde to confirm the occurrence of Es in the statistics. This implies that some of the samples of HFD data in the statistics might have not represented the characteristics of Es, which is the possible reason for the more scattered Es samples in the statistical results.

In Fig. 6a and b, we directly compared the propagation direction and speed of Es and MSTIDs that appeared on the same magnetic flux tube. The total number of events was only 68, which is primarily due to the lack of the coverage of GPS receivers in the sea area. We need to use 2 h of HFD and GPS-TEC data for calculating the propagation parameters through cross-correlation. However, all the green points in Fig. 2 are located in the sea area, where the GPS-TEC data are often unavailable, for longer than 1 h in the worst case. This lack of GPS-TEC data reduced the number of points in the statistics and affected its statistical significance. In Fig. 6b, the propagation speeds of MSTIDs tend to be higher as compared to those in Fig. 5b. The reason for this increase in the speed of MSTIDs is unclear although slightly coarser data

coverage of GPS-TEC in the sea area might have affected the velocity estimation. However, the propagation speeds of MSTIDs in Fig. 6b are closer to those of Es in comparison with Fig. 5b, suggesting that further stronger correlation is observed between the E and F regions when considering the field line mapping.

Although there was some scattering in the propagation direction and speed in Fig. 6a and b, the statistical results were generally consistent with those in Fig. 5a and b. The overall matching of the propagation parameters of Es and MSTIDs is still prominent even if we employ the data from different regions at two different altitudes connected via magnetic field line. This study assumed that the wavefronts of Es and MSTIDs have a plain wave structure extending for a long distance (Kurihara et al. 2010; Tsugawa et al. 2007). Such an elongating structure of MSTIDs, which is clearly shown in the attached Additional file 1: Movie S1 of dTEC map, can be detected even if the TEC data are obtained at points slightly different from the actual conjugate point of Es; thus, the overall agreement between the propagation characteristics of Es and MSTIDs is shown in Fig. 5.

Figure 7 shows the dependence of the propagation parameters on local time. In Fig. 7a, it is indicated that the number of events is smaller in the earlier and later JST intervals, in particular, before 20 JST and after 01 JST. We speculate that this is because the wave-like structures of Es or MSTIDs have not yet clearly been formed in those LT intervals. In this study, we processed the data from 18 to 03 JST. However, no wave-like signatures were detected before 18 JST, supporting the speculation mentioned above. Yokoyama et al. (2009) demonstrated by using the

numerical simulation that the Perkins instability (Perkins 1973) and the Es layer instability (Cosgrove and Tsunoda 2002, 2003) have an important effect on the generation of Es and MSTIDs. In earlier LT intervals, there are a small number of events in those periods because this process is not working well enough yet. On the other hand, the low number of events after 01 JST is considered to be due to the smaller inhomogeneity of the plasma density in the E region, which causes a weaker contribution of MSTIDs to forming the wavefronts (Otsuka et al. 2008).

Figure 7b and c, respectively, shows the LT variation of the averaged propagation parameters. The averaged parameters are plotted every 15 min which is equal to the temporal resolution of foEs from the ionosonde used for the detection of Es. The red circles show the averaged parameter of Es and the blue circles show that of MSTIDs. It can be noted that the parameters of Es and MSTID are almost the same for both the propagation speed and propagation direction. Particularly, the propagation directions of Es and MSTIDs are southwestward for almost all the time period. Considering the tidal wind, the neutral wind changes in a clockwise direction near the altitude where Es is generated. Therefore, Es formed by shear is propagated southward by the southward neutral wind. However, because the wavefront is formed in the northwest-southeast direction, it apparently propagates in the southwest direction (Yokoyama et al. 2009). The results in Fig. 7 clearly show this tendency.

Figure 7c also confirms that MSTIDs, shown by the red points, also propagate in the southwest direction, the propagation azimuth being between 180° and 270°. This is consistent with the E–F coupling model in which the formation of MSTIDs in the F region is closely affected by Es in the E region and propagate in tandem due to electric coupling via magnetic field lines. Figure 7c also shows that the propagation azimuth of both Es and MSTIDs increases gradually with time. This means that the propagation direction is shifting from the southwest to west, i.e., the elongation of wavefront is getting more perpendicular to the east–west direction.

When considering the wavefronts of MSTIDs in the framework of Perkins instability, it is important to determine the direction of the electric current in the F region (~300 km), which is expressed by the following equation:

$$\mathbf{J} = \Sigma(\mathbf{E} + \mathbf{U} \times \mathbf{B}), \quad (3)$$

where Σ is the field line-integrated conductivity, \mathbf{E} is the background electric field, \mathbf{U} is the neutral wind, and \mathbf{B} is the magnetic field. In the mid-latitude nighttime F region, \mathbf{E} is generated by the F region dynamo, so that \mathbf{E} is opposite direction to $\mathbf{U} \times \mathbf{B}$ and $|\mathbf{U} \times \mathbf{B}|$ is larger than $|\mathbf{E}|$. Therefore, \mathbf{J} flows in the direction of $\mathbf{U} \times \mathbf{B}$. Considering the Perkins instability, when the direction of the

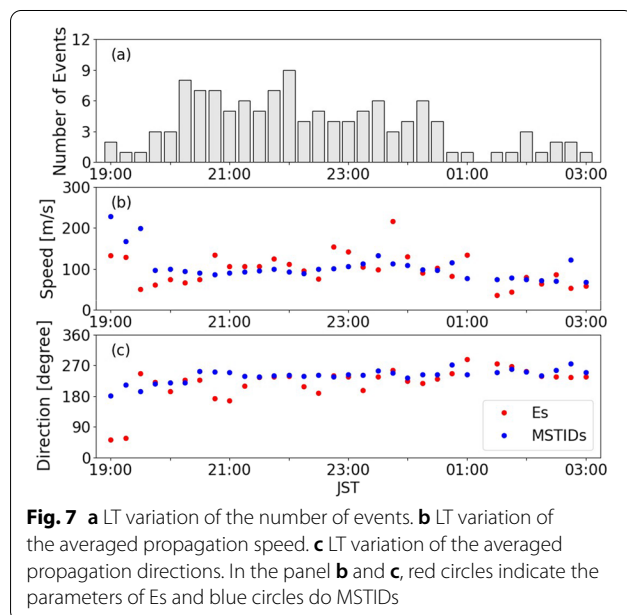


Fig. 7 a LT variation of the number of events. b LT variation of the averaged propagation speed. c LT variation of the averaged propagation directions. In the panel b and c, red circles indicate the parameters of Es and blue circles do MSTIDs

wave vector \mathbf{k} is between the east–west direction and \mathbf{J} , the instability grows (Perkins 1973). The neutral wind \mathbf{U} in the F region (~ 300 km) changes from southeast to south (HWM: Drob et al. 2015) during the local time interval considered here; thus, \mathbf{J} changes accordingly from northeast to east. Correspondingly, the direction of the wave vector \mathbf{k} also changes in a clockwise direction. This means that the wavefront of MSTIDs should become more perpendicular to the east–west direction under the influence of the local time variation of the background neutral wind. The similar change in the wavefront direction of Es would be due to the influence of the F region electrodynamics transferred along the magnetic field lines on the structure in the E region. In such senses, Es and MSTIDs influence each other and determine their propagation direction in the E–F region coupled system.

Shiokawa et al. (2003) conducted observations of MSTIDs using all-sky airglow imagers at Rikubetsu (43.5°N , 143.8°E) and Shigaraki (34.8°N , 136.1°E) in Japan, and performed a statistical analysis of MSTIDs using 2 years of data. They demonstrated that the propagation direction of MSTIDs during summer nighttime was southwest and the propagation speed ranges from 50 to 100 m/s. The propagation speed and direction of MSTIDs in our statistics are fairly consistent with those of Shiokawa et al. (2003). In this study, the propagation characteristics of Es were also statistically analyzed at the same time, and it was shown that the propagation parameters of Es are very close to those of MSTIDs. This result strongly supports the formation of wave-like structure (i.e., Es and MSTIDs) at two different altitudes through E–F coupling mechanism.

Studies of E–F coupling process include the simultaneous observation of MSTIDs in the F region and quasi-periodic (QP) echoes (Yamamoto et al. 1991) in the E region. Yamamoto et al. (1994) indicated that the QP echo had wavefronts extending from northwest to southeast and propagated southwestward at a speed of slightly faster than 100 m/s. Saito et al. (2007) conducted simultaneous observations of QP echoes by the MU radar and MSTIDs by GPS-TEC. Their results demonstrated that the band structure of QP echoes and MSTIDs were aligned from northwest to southeast, and they propagated to the southwest. Otsuka et al. (2007) showed that the period of the Doppler velocity variation in the QP echoes was very similar to that of MSTIDs observed in the airglow measurement. Furthermore, the increase or decrease of the airglow intensity within MSTIDs is closely related to the direction of the Doppler velocity of the QP echoes. These results strongly imply that

the electrodynamic coupling between Es and F region could play an important role in generation and characterization of Es structures and MSTIDs.

The generation of MSTIDs through the E–F coupling mechanism has been supported by several theoretical studies (Cosgrove and Tsunoda 2002, 2004) and numerical simulations (Yokoyama et al. 2009; Yokoyama and Hysell 2010). However, simultaneous observations of propagation characteristics in the E and F regions using a large amount of data have not been made in the past. We have conducted for the first time a statistical analysis of the propagation characteristics of Es and MSTIDs based on simultaneous observations of two different altitudes. The results support the E–F coupling theory for the generation of MSTIDs. However, we only investigated the overall propagation characteristics of both the phenomena and have not yet their spatial characteristics, for example, period and wavelength. By comparing the black lines of Fig. 3a and b, we can find that the HFD observation captures the structure of Es at the same level as the horizontal wavelength of MSTIDs. We plan to focus our analysis on the spatial structure of Es and MSTIDs, especially their wavelengths and periodicity.

Summary and conclusion

In this study, we derived the horizontal propagation speed and direction of Es and MSTIDs from multi-point observations of HF Doppler sounder and GPS-TEC. During a case of Es/MSTIDs on the night of August 22, 2014, the propagation speed and direction of Es were 68.9 m/s and 247° , respectively, while those of MSTIDs were 68.1 m/s and 250° . The statistics using 122 Es/MSTID cases in four years from 2014 to 2017 also confirmed that Es and MSTIDs propagated together with similar direction and speed in most of the events. The propagation direction of Es and MSTID was southwest and the speed was 50–100 m/s, which is consistent with the characteristics of summer nighttime MSTIDs. This “in tandem” motion of Es and MSTIDs supports the generation of wave-like structures in both the E and F region ionosphere through the electric coupling of two instabilities at two different altitudes. This is the first statistical analysis comparing the motion of Es and MSTID based on the simultaneous observations at two altitudes although there were studies showing similar relationship using QP echoes as a manifestation of Es. The current approach of using HFD for observing the motion of Es will allow us to investigate the dynamical characteristics of the small-scale structures in the summer nighttime E region ionosphere.

Abbreviations

Es: Sporadic E; HF: High frequency; VHF: Very high frequency; TEC: Total electron content; MSTIDs: Medium-scale traveling ionospheric disturbances; HFD: High-frequency Doppler; GPS: Global positioning system; GNSS: Global navigation satellite system; GEONET: GNSS Earth observation network system; GPS-TEC: TEC obtained from the GPS receivers of GEONET; AGWs: Atmospheric gravity waves; FFT: Fast Fourier transform; JST: Japan standard time; NIPR: National Institute of Polar Research; dTEC: Detrended vertical TEC; TECU: TEC unit; NICT: National Institute of Information and Communications; LT: Local time; QP: Quasi-periodic.

Supplementary Information

The online version contains supplementary material available at <https://doi.org/10.1186/s40623-022-01616-3>.

Additional file 1: Movie S1. An example of mapping of MSTIDs over Japan by using dTEC of GEONET for 2.5 h from 2300 to 2530 JST on August 21, 2021. The color represents the dTEC value in each grid derived every 30 s.

Acknowledgements

The operation of the receivers at Oarai has been supported by the National Institute of Information and Communications Technology (NICT).

Author contributions

RM designed and executed the study and wrote the manuscript. KH and JS provided assistance in the conduct of the study. YM assisted in the interpretation of the E–F coupling. MKE conducted the Lidar observations of the Ca⁺ layer and helped interpret the results. MN and TT observed TEC and contributed to the research methodology. All the authors read and approved the final manuscript.

Funding

The HFD project in Japan is supported by the Takahashi Industrial and Economic Research Foundation (FY2019, FY2020), Murata Science Foundation (FY2020), and Hosono Bunka Foundation (FY2019).

Availability of data and materials

In this study, we used the GPS-TEC data provided by the DRAWING-TEC database (<https://aer-nc-web.nict.go.jp/GPS/DRAWING-TEC/>). We employed data from the HFD system currently in operation in Japan (HFDOPE: <http://gwave.cei.uec.ac.jp/~hfd>). Ionosonde data were provided by WDC for Ionosphere and Space Weather, Tokyo, National Institute of Information and Communications Technology (http://wdc.nict.go.jp/IONO/index_E.html).

Declarations

Ethics approval and consent to participate

Not applicable.

Consent for publication

Not applicable.

Competing interests

The authors declare that they have no competing interests.

Author details

¹University of Electro-Communications, Chofugaoka 1-5-1, Chofu, Tokyo 182-8585, Japan. ²Institute for Space-Earth Environment Research, Nagoya University, Furocho F3-3, Chikusa-ku, Nagoya, Aichi 464-8601, Japan. ³National Institute of Polar Research, 10-3, Midoricho, Tachikawa, Tokyo 190-8518, Japan. ⁴Department of Polar Science, SOKENDAI (The Graduate University for Advanced Studies), 10-3, Midoricho, Tachikawa, Tokyo 190-8518, Japan. ⁵National Institute of Information and Communications Technology, Nukui-Kitamachi 4-2-1, Koganei, Tokyo 184-8795, Japan.

Received: 2 December 2021 Accepted: 31 March 2022

Published online: 24 April 2022

References

- Cosgrove RB, Tsunoda RT (2002) A direction-dependent instability of sporadic E layers in the nighttime midlatitude ionosphere. *Geophys Res Lett* 29(18):11-1-11-4. <https://doi.org/10.1029/2002gl014669>
- Cosgrove RB, Tsunoda RT (2003) Simulation of the nonlinear evolution of the sporadic-E layer instability in the nighttime midlatitude ionosphere. *J Geophys Res Space Phys.* <https://doi.org/10.1029/2002JA009728>
- Cosgrove RB, Tsunoda RT (2004) Instability of the E–F coupled nighttime midlatitude ionosphere. *J Geophys Res Space Phys.* <https://doi.org/10.1029/2003JA010243>
- Drob DP, Emmert JT, Meriwether JW, Makela JJ, Doornbos E, Conde M, Hernandez G, Noto J, Zawdie KA, McDonald SE, Huba JD, Klenzing JH (2015) An update to the Horizontal Wind Model (HWM): the quiet time thermosphere. *Earth Space Sci* 2(7):301–319. <https://doi.org/10.1002/2014EA000089>
- Ejiri MK, Nakamura T, Tsuda TT, Nishiyama T, Abo M, She CY, Nishioka M, Saito A, Takahashi T, Tsuno K, Kawahara TD, Ogawa T, Wada S (2019) Observation of synchronization between instabilities of the sporadic E layer and geomagnetic field line connected F region medium-scale traveling ionospheric disturbances. *J Geophys Res Space Phys* 124(6):4627–4638. <https://doi.org/10.1029/2018JA026242>
- Haldoupis C (2011) A tutorial review on sporadic E layers. *Aeron Earths Atmos Ionos.* <https://doi.org/10.1007/978-94-007-0326-1>
- Haldoupis C, Pancheva D, Singer W, Meek C, MacDougall J (2007) An explanation for the seasonal dependence of midlatitude sporadic E layers. *J Geophys Res Space Phys.* <https://doi.org/10.1029/2007JA012322>
- Helmboldt J (2016) A multi-platform investigation of midlatitude sporadic E and its ties to E–F coupling and meteor activity. *Ann Geophys* 34(5):529–541. <https://doi.org/10.5194/angeo-34-529-2016>
- Hines CO (1960) Internal atmospheric gravity waves at ionospheric heights. *Can J Phys.* <https://doi.org/10.1139/p60-150>
- Hooke WH (1968) Ionospheric irregularities produced by internal atmospheric gravity waves. *J Atmos Terr Phys* 30(5):795–823. [https://doi.org/10.1016/S0021-9169\(68\)80033-9](https://doi.org/10.1016/S0021-9169(68)80033-9)
- Hunsucker R (1982) Atmospheric gravity waves generated in the high-latitude ionosphere: a review. *Rev Geophys* 20(2):293–315. <https://doi.org/10.1029/RG020i002p00293>
- Hysell DL, Yokoyama T, Nossa E, Hedden RB, Larsen MF, Munro J, Smith S, Sulzer MP, Gonzalez SA (2011) Radar and optical observations of irregular midlatitude sporadic E layers beneath MSTIDs. *Aeron Earths Atmos Ionos* 2:269–281. https://doi.org/10.1007/978-94-007-0326-1_19
- Kurihara J, Koizumi-Kurihara Y, Iwagami N, Suzuki T, Kumamoto A, Ono T, Nakamura M, Ishii M, Matsuoka A, Ishisaka K, Abe T, Nozawa S (2010) Horizontal structure of sporadic E layer observed with a rocket-borne magnesium ion imager. *J Geophys Res Space Phys.* <https://doi.org/10.1029/2009JA014926>
- Maeda J, Heki K (2014) Two-dimensional observations of midlatitude sporadic E irregularities with a dense GPS array in Japan. *Radio Sci* 49(1):28–35. <https://doi.org/10.1002/2013RS005295>
- Maeda J, Heki K (2015) Morphology and dynamics of daytime mid-latitude sporadic-E patches revealed by GPS total electron content observations in Japan. *Earth Planets Space* 67:89. <https://doi.org/10.1186/s40623-015-0257-4>
- Muafiry IN, Heki K, Maeda J (2018) 3D tomography of midlatitude sporadic-E in Japan from GNSS-TEC data. *Earth Planets Space* 70:45. <https://doi.org/10.1186/s40623-018-0815-7>
- Narayanan VL, Shiokawa K, Otsuka Y, Saito S (2006) Airglow observations of nighttime medium-scale traveling ionospheric disturbances from Yonaguni: statistical characteristics and low-latitude limit. *J Geophys Res Space Phys* 119(11):9268–9282. <https://doi.org/10.1002/2014JA020368>
- Ogawa T, Nishitani N, Otsuka Y, Shiokawa K, Tsugawa T, Hosokawa K (2009) Medium-scale traveling ionospheric disturbances observed with the SuperDARN Hokkaido radar, all-sky imager, and GPS network and their relation to concurrent sporadic E irregularities. *J Geophys Res Space Phys.* <https://doi.org/10.1029/2008JA013893>
- Otsuka Y, Onoma F, Shiokawa K, Ogawa T, Yamamoto M, Fukao S (2007) Simultaneous observations of nighttime medium-scale traveling ionospheric disturbances and E region field-aligned irregularities at midlatitude. *J Geophys Res Space Phys.* <https://doi.org/10.1029/2005JA011548>
- Otsuka Y, Tani T, Tsugawa T, Ogawa T, Saito A (2008) Statistical study of relationship between medium-scale traveling ionospheric disturbance and

- sporadic E layer activities in summer night over Japan. *J Atmos Solar Terr Phys* 70(17):2196–2202. <https://doi.org/10.1016/j.jastp.2008.07.008>
- Otsuka Y, Kotake N, Shiokawa K, Ogawa T, Tsugawa T, Saito A (2011) Statistical study of medium-scale traveling ionospheric disturbances observed with a GPS receiver network in Japan. *Aeron Earths Atmos Ionos* 2:291–299. https://doi.org/10.1007/978-94-007-0326-1_21
- Otsuka Y, Suzuki K, Nakagawa S, Nishioka M, Shiokawa K, Tsugawa T (2013) GPS observations of medium-scale traveling ionospheric disturbances over Europe. *Ann Geophys* 31(2):163–172. <https://doi.org/10.5194/angeo-31-163-2013>
- Park J, Lühr H, Min KW, Lee JJ (2010) Plasma density undulations in the night-time mid-latitude F-region as observed by CHAMP, KOMPSAT-1, and DMSP F15. *J Atmos Solar Terr Phys* 72(2–3):183–192. <https://doi.org/10.1016/j.jastp.2009.11.007>
- Perkins F (1973) Spread F and ionospheric currents. *J Geophys Res* 78(1):218–226. <https://doi.org/10.1029/ja078i001p00218>
- Saito A, Fukao S, Miyazaki S (1998) High resolution mapping of TEC perturbations with the GSI GPS network over Japan. *Geophys Res Lett* 25(16):3079–3082. <https://doi.org/10.1029/98GL52361>
- Saito S, Yamamoto M, Hashiguchi H, Maegawa A, Saito A (2007) Observational evidence of coupling between quasi-periodic echoes and medium scale traveling ionospheric disturbances. *Ann Geophys* 25(10):2185–2194. <https://doi.org/10.5194/angeo-25-2185-2007>
- Sakai J, Hosokawa K, Tomizawa I, Saito S (2019) A statistical study of anomalous VHF propagation due to the sporadic-E layer in the air-navigation band. *Radio Sci* 54(5):426–439. <https://doi.org/10.1029/2018RS006781>
- Sakai J, Saito S, Hosokawa K, Tomizawa I (2020) Anomalous propagation of radio waves from distant ILS localizers due to ionospheric sporadic-E. *Space Weather*. <https://doi.org/10.1029/2020SW002517>
- Shiokawa K, Ihara C, Otsuka Y, Ogawa T (2003) Statistical study of nighttime medium-scale traveling ionospheric disturbances using midlatitude airglow images. *J Geophys Res Space Phys*. <https://doi.org/10.1029/2002JA009491>
- Thébault E, Finlay CC, Beggan CD, Alken P, Aubert J, Barrois O, Bertrand F, Bondar T, Boness A, Brocco L, Canet E, Chambodut A, Chulliat A, Coisson P, Civet FD, Du A, Fournier A, Fratter I, Gillet N, Hamilton B, Hamoudi M, Hulot G, Jager T, Korte M, Kuang ZT (2015) International Geomagnetic Reference field: the 12th generation. *Earth Planets Space*. <https://doi.org/10.1186/s40623-015-0228-9>
- Tsugawa T, Kotake N, Otsuka Y, Saito A (2007) Medium-scale traveling ionospheric disturbances observed by GPS receiver network in Japan: a short review. *GPS Solut* 11:139–144. <https://doi.org/10.1007/s10291-006-0045-5>
- Vincent RA, Reid IM (1983) HF doppler measurements of mesospheric gravity wave momentum fluxes. *J Atmos Sci* 40(5):1321–1333. [https://doi.org/10.1175/1520-0469\(1983\)040%3C1321:HDMOMG%3E2.0.CO;2](https://doi.org/10.1175/1520-0469(1983)040%3C1321:HDMOMG%3E2.0.CO;2)
- Watts JM, Davies K (1960) Rapid frequency analysis of fading radio signals. *J Geophys Res* 65(8):2295–2301. <https://doi.org/10.1029/JZ065i008p02295>
- Whitehead JD (1961) The formation of sporadic-E layers in the temperate zones. *J Atmos Terr Phys* 20(1):49–58. [https://doi.org/10.1016/0021-9169\(61\)90097-6](https://doi.org/10.1016/0021-9169(61)90097-6)
- Yamamoto M, Fukao S, Woodman RF, Ogawa T, Tsuda T, Kato S (1991) Mid-latitude E region field-aligned irregularities observed with the MU Radar. *J Geophys Res Space Phys* 96(A9):15943–15949. <https://doi.org/10.1029/91JA01321>
- Yamamoto M, Komoda N, Fukao S, Tsunoda RT, Ogawa T, Tsuda T (1994) Spatial structure of the E region field-aligned irregularities revealed by the MU radar. *Radio Sci* 29(1):337–347. <https://doi.org/10.1029/93RS01846>
- Yokoyama T, Hysell DL (2010) A new midlatitude ionosphere electrodynamics coupling model (MIECO): latitudinal dependence and propagation of medium-scale traveling ionospheric disturbances. *Geophys Res Lett*. <https://doi.org/10.1029/2010GL042598>
- Yokoyama T, Hysell DL, Otsuka Y, Yamamoto M (2009) Three-dimensional simulation of the coupled Perkins and Es-layer instabilities in the night-time midlatitude ionosphere. *J Geophys Res Space Phys*. <https://doi.org/10.1029/2008JA013789>

Publisher's Note

Springer Nature remains neutral with regard to jurisdictional claims in published maps and institutional affiliations.

Submit your manuscript to a SpringerOpen[®] journal and benefit from:

- Convenient online submission
- Rigorous peer review
- Open access: articles freely available online
- High visibility within the field
- Retaining the copyright to your article

Submit your next manuscript at ► [springeropen.com](https://www.springeropen.com)